Supporting information for

Investigations of Low Frequency Vibrational Dynamics and Ligand Binding Kinetics of Cystathionine β-synthase

*Venugopal Karunakaran[†], Abdelkrim Benabbas[†], Yuhan Sun[†], Zhenyu Zhang[†], Sangita Singh[§], Ruma Banerjee[§], Paul M. Champion[†]**

[†]Department of Physics and Center for Interdisciplinary Research on Complex Systems, Northeastern University, Boston, Massachusetts 02115, USA, [§]Department of Biological Chemistry, University of Michigan, Ann Arbor, MI 4810,USA.

p.champion@neu.edu

Experimental details for vibrational coherence spectroscopy

The laser system used for the degenerate pump-probe coherence experiments consists of a tunable (750–960 nm) Ti-Sapphire oscillator (MIRA 900; Coherent, Santa Clara, CA) pumped by a diode laser (Verdi 10; Coherent). The oscillator is able to generate pulses of 50–100 fs, 76 MHz with energy of ~10 nJ/pulse. The pulses were frequency-doubled in a 250 μm β-barium borate crystal and then chirp-compensated by a pair of SF10 prisms. Subsequently, the laser light was split with a ratio of 2:1 for the pump and probe beams respectively. The pump beam was modulated using an acousto-optic modulator (NEOS Technologies, Melbourne, FL) at 1.5 MHz. Before entering the sample, the pump and probe beam polarizations were adjusted to be perpendicular to one another. The time delay between the pump and probe pulse was controlled by a Klinger translation stage (Newport, Irvine, CA). After the sample, the beams were recollimated and the pump light was spatially blocked (using a pinhole) and extinguished by a polarization analyzer that only allowed the probe light to pass.

Preparation of the ferrous NO bound form of CBS

When preparing the ferrous NO bound sample for measurements, we added an excess of $Na_2S_2O_4$ so that the dithionite peak near 320 nm was about two times that of the Soret band. Then $NaNO_2$ was added and the reaction with $Na_2S_2O_4$ generated the NO complex with a fairly rapid loss of the 320nm peak. Following the coherence experiment, a new peak appeared near 426 nm, suggesting that some re-oxidation takes place, perhaps due to trace O_2 contamination. (The absorption spectra of the NO complex before and after the FCS experiments is shown in Fig. S1. Further studies show that the 426 nm peak is due to oxidized material and that upon reduction the sample partially reverts to the 448 nm species as reported previously[1].

According to prior work [2], binding of NO to the ferrous form of CBS leads to a 5-coordinate Fe^{2+}-NO species. However, the absorption spectrum of the ferrous NO sample is noticeably altered following the measurement (Fig. S1 shows the spectrum following 4 h of laser irradiation) and a shoulder appears near 426nm that is suggestive of re-oxidation. Further studies reveal that exposure to oxygen leads to rapid, but incomplete, re-oxidation of the ferrous NO species. It appears that resonance enhancement at the probe wavelength of 425 nm leads to a predominant ferric CBS coherence spectrum (see Fig. 5A). Additional studies utilizing significantly blue-shifted probe wavelengths will be necessary in order to study the ferrous CBS-NO coherence spectrum.

NSD Analysis.

The NSD analysis determines the geometric distortions of the heme when it is exposed to different protein environments. We use the planar structure of ferric porphine, [Fe(P)]+ as a reference, derived from DFT optimization under D_{4h} symmetry, and we include the iron as well as the 24 skeletal atoms. Each displacement along normal coordinate $\boldsymbol{Q}_\alpha$ is determined in the mass-weighted coordinate space using the scalar product $(\boldsymbol{X} - \boldsymbol{X_0}) \cdot \boldsymbol{Q}_\alpha$, where $\boldsymbol{X}$ and $\boldsymbol{X_0}$ are the mass-weighted atomic coordinates of the input and reference structures, respectively. The quantity $\boldsymbol{Q}_\alpha$ is the unit vector of the mass-weighted normal mode, α, of the reference structure $[Fe(P)]^+$. The difference between the structures is found by a least-squares superposition of the structures using a Swiss-PdbViewer (ver. 3.7) [3]. Thus, we can find the displacements along low frequency out-of-plane (OOP) modes of different symmetry (such as propellering, ruffling, saddling, waving*(x)*, waving*(y)*, doming and inverse doming) and use them to describe the observed heme structure. We include both the doming (Fe moves with the porphine nitrogens) and the inverse doming (Fe motion opposite to porphine nitrogens) modes to more accurately specify the iron OOP position, which is approximately the sum of these displacements. A

negative displacement is defined only for these two modes, where it indicates the direction of the iron OOP movement (+ is proximal and - is distal).

Analysis of CO rebinding kinetics to CBS and CooA using the SRC model

In contrast to CBS, the gene activator protein CooA from the bacterium *Rhodospirillum rubrum* has been found to display a positive cooperativity for CO[4]. In the dimeric CooA protein, CO binds and replaces an N-terminal amine group belonging to a proline residue. For CooA the successive CO equilibrium constants are 0.17 and 1.25 μM^{-1} for the first and second binding steps[4], while the dimer of truncated CBS exhibits equilibrium constants of 0.24 and 0.02 μM^{-1}. Likewise, the rate constant for endogenous ligand (Cys 52) dissociation, 0.0166 s^{-1}, is lower for CBS than for the prolines in CooA (0.2 and 0.07 s^{-1})[5]. The geminate recombination of CO in CooA has also been studied previously in the visible[6] and mid-infrared region[7] and found to occur on the sub-nanosecond time scale with a high geminate yield.

As can be seen in Fig. 10A, the geminate recombination of CO to both CooA and truncated CBS is non-exponential. To describe the kinetic responses we used a model based on a distribution of heme doming conformations, which has been described in detail by Srajer, Reinish and Champion (SRC)[8;9]. Within this model the enthalpic barrier for CO binding is separated into two parts

$$H = H_p(a) + H_0 = \frac{1}{2}Ka^2 + H_0 \ . \qquad (1)$$

H_p represents the proximal barrier due the heme doming and, *a*, is the protein conformation-dependent generalized iron out-of-plane equilibrium position. K is the effective force constant along the doming coordinate and H_0 represents the remaining (mostly distal) contributions to the barrier; it contains energies involving ligand docking sites and steric constraints associated with the distal pocket as well

as an *a*-independent term from the linearly coupled heme potential surface[8]. We assume that the distribution of the iron out-of-plane displacements, *P(a)*, is Gaussian with a_0 representing the average out-of-plane displacement in the unbound state, and σ_a its variance. Using *P(a)* a distribution for the barrier heights *g(H)* can be calculated[8;9] and the survival population at time t after photolysis can be written as,

$$N(t) = \int_{H_0}^{\infty} g(H) e^{-k(H)t} dH \tag{2a}$$

with

$$k(H) = k_1 \exp\left(\frac{-H_p(a)}{k_B T}\right) \tag{2b}$$

and

$$k_1 = k_0 \exp\left(\frac{-H_0}{k_B T}\right) \quad . \tag{2c}$$

N(t) can be evaluated as

$$N(t) = I_g \int_0^{\infty} dx \frac{A}{2\sqrt{\pi x}} \left(e^{-\left(A\sqrt{x}-C\right)^2} + e^{-\left(A\sqrt{x}+C\right)^2} \right) e^{-k_1 t\, e^{-x}} + (1 - I_g) \tag{3}$$

Where the parameter I_g represents the geminate amplitude. Equation (3) is valid when the value of the geminate amplitude I_g is near unity, which is the case for both CooACO and CBSCO. The fundamental parameters $\{a_0, \sigma_a\}$ that describe the heme conformational distribution can be calculated from the fitting parameters $\{A, C\}$ as,

$$\sigma_a = \sqrt{\frac{k_B T}{K A^2}} \tag{4a}$$

$$a_0 = \sqrt{\frac{2k_B T}{K}}\left(\frac{C}{A}\right) \tag{4b}$$

Equation (3) fits the CooA-CO data very well, but it does not correctly fit the kinetic response of CBS-CO. When stretched exponentials were used we could obtain a reasonable fit, but we found this unsatisfying from an interpretive perspective. As a result, we attempted fits using an extended version of the SRC model, where we invoke the assumption that the two subunit sites might show different CO kinetics. If all parameters are allowed to be free in a two-site version of the SRC model, the fit is underdetermined. We therefore held the amplitudes and widths, σ_a , of the subunit distributions equal.

The formal expression for the sum of the two (noted as i=1,2) equally weighted SRC distributions is given as :

$$N(t) = I_g \int_0^\infty dx \frac{A_1}{2\sqrt{\pi x}}\left(e^{-\left(A_1\sqrt{x}-C_1\right)^2} + e^{-\left(A_1\sqrt{x}+C_2\right)^2}\right)e^{-k_{11}te^{-x}} + I_g \int_0^\infty dx \frac{A_2}{2\sqrt{\pi x}}\left(e^{-\left(A_2\sqrt{x}-C_2\right)^2} + e^{-\left(A_2\sqrt{x}+C_2\right)^2}\right)e^{-k_{12}te^{-x}} + (1-2I_g) \tag{5}$$

The widths converged near 0.1 Å and the centroids were near a_0~0.3 Å for both subunits, as found for other heme systems studied with this model. The fitting parameters for both CooA-CO and CBS-CO are displayed in Table 4 of the manuscript.

As mentioned above, we attribute the additional kinetic heterogeneity in CBS to the fact it is a dimer with two inequivalent binding sites. In fact it has been shown that CO binding to truncated CBS has two successive association constants[5] : 0.24 and 0.02 μM^{-1}. However the measurement of the on-rate of CO in truncated CBS is limited by Cys dissociation and is found[5] to be $k_{on} = 18 \pm 4\ \mu M^{-1}s^{-1}$ for both subunits.

We show below that the ratio of the intrinsic geminate rates for CO rebinding in the two sub-units of CBS, extracted using equation 4, is in good agreement with the ratio of the two association constants measured in ref 3. In order to estimate the intrinsic geminate rate of the two binding sites we use a simple three state model[10;11] for each subunit (i=1.2), assuming that the k_{BA}^{i} can be approximated by the SRC average rate $\langle k_{BA} \rangle_i$:

$$CBS_i CO \underset{\langle k_{BA} \rangle_i}{\overset{k_{AB}^{i}}{\rightleftarrows}} CBS_i : CO \underset{k_{in}^{i}}{\overset{k_{out}^{i}}{\rightleftarrows}} CBS_i + CO \qquad (6)$$

Where $i = 1,2$ is referring to the two sub-units of the CBS dimer.

The SRC average rate can be written as

$$\langle k_{BA} \rangle_i = \int k_i(H) g_i(H) dH = \int k_i(a) P_i(a) da = k_{1i} \int \exp\left(-\frac{H_{pi}(a)}{k_B T} \right) P_i(a) da \qquad (7)$$

The ratio of the intrinsic geminate rates of the two binding sites can then be approximated as:

$$\frac{k_{BA}^{1}}{k_{BA}^{2}} \approx \frac{\langle k_{BA} \rangle_1}{\langle k_{BA} \rangle_2} \approx \frac{k_{11}}{k_{12}} = 21, \qquad (8)$$

In equation (8) we use the fact that $P_1(a) \sim P_2(a)$ (see Table 4) so that the term under integral in Equation (7) is the same for both sites. If we further assume that the Arrhenius prefactor k_0 is the same for both binding sites, then Eq. 2c with T= 300K yields:

$$H_{02} - H_{01} = k_B T \ln(21) = 7.3 \text{ kJ/mole},$$

which is similar to the "distal" barrier found[8] for Mb, where H_0 = 7kJ/mol.

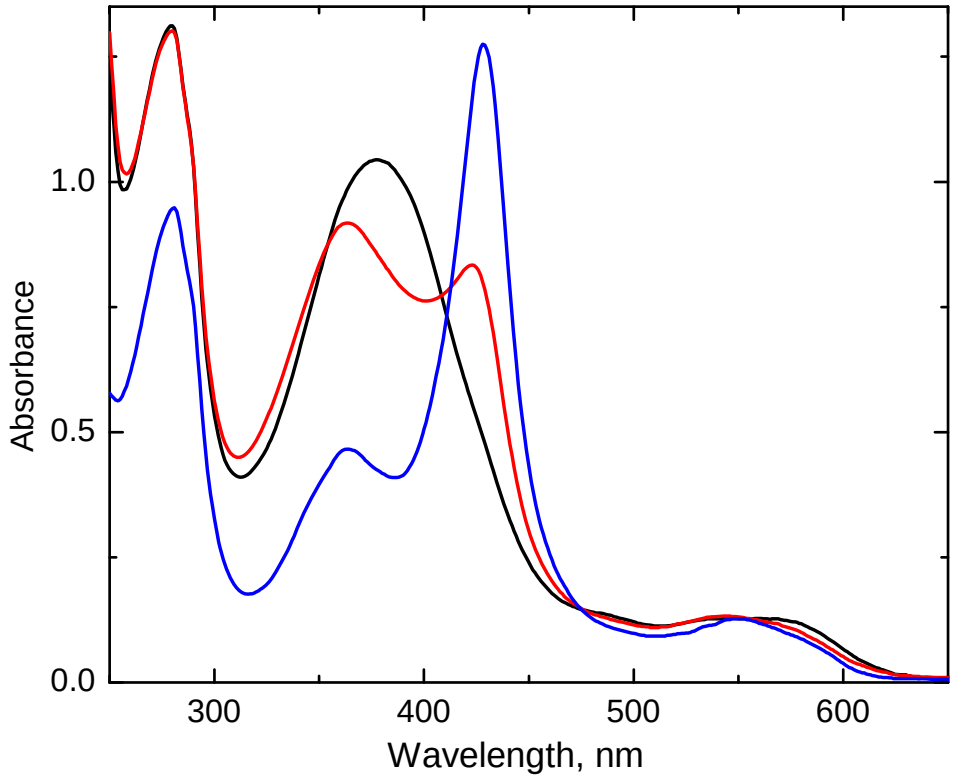

Figure S1 Absorption spectra of ferrous CBS-NO complex at pH 8: before (black) and after (red) the vibrational coherence spectroscopy measurements. The shoulder around 426 nm (red) shows evidence of re-oxidation to ferric CBS. The absorption spectra of ferric CBS at pH 8 is also shown for comparison (blue).

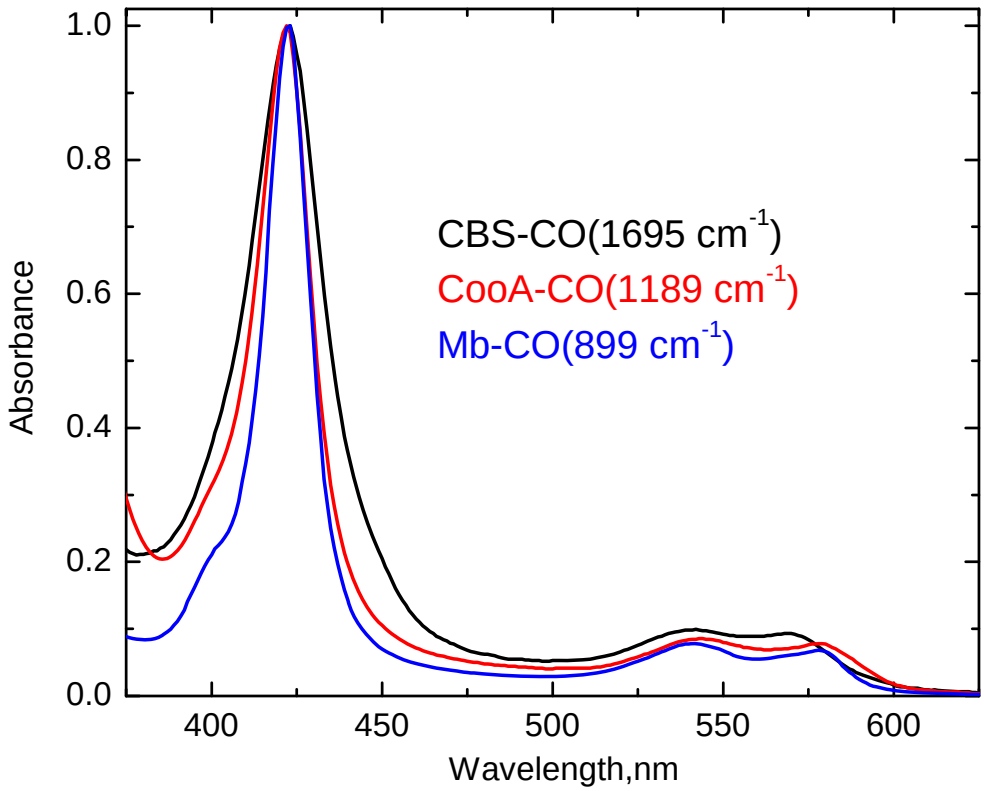

Figure S2 Absorption spectra of the CO complex of various heme proteins: CBS (black), CooA (red) and myoglobin (blue) and their full width at half maximum (FWHM) values are shown in parenthesis. The larger FWHM for CBS-CO suggests that inhomogeniety is present, which may account for the differences between CO binding in the dimeric structures.

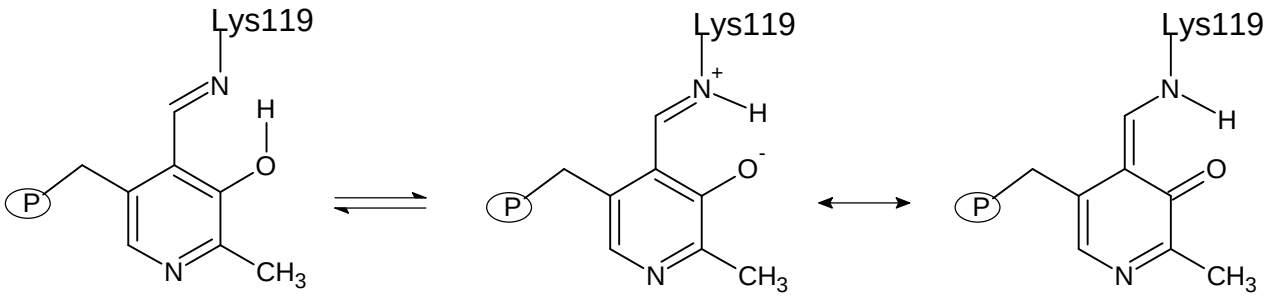

Enolimine Ketoenamine

Figure S3 Tautomeric equilibrium of PLP between ketoenamine and enolimine in CBS

Tables of rates and amplitudes corresponding to the fits in Fig. 2B, Fig. 5B, and Fig. 7B

Table S1 Time constants and amplitudes for the population dynamics of ferric CBS at pH 8.

λ_{ex} (nm)	Decay time (ps)	Amplitude
412	0.18(τ_1)	129.92(a_1)
	0.69(τ_2)	-29.92(a_2)
425	0.14(τ_1)	47.82(a_1)
	0.59(τ_2)	23.45(a_2)
	3.78(τ_3)	28.57(a_3)
432	0.35(τ_1)	28.53(a_1)
	0.62(τ_2)	14.50(a_2)
	0.97(τ_3)	56.97(a_3)
443	0.77(τ_1)	167.20(a_1)
	3.32(τ_2)	-67.20(a_2)

Table S2 Lifetimes and amplitudes for the population dynamics of CBS in the ferric, ferrous, and ferrous NO states at pH 8.

Complex	Decay time (ps)	Amplitude
Fe^{3+}	0.140(τ_1)	47.82(a_1)
	0.593(τ_2)	23.45(a_2)
	3.784(τ_3)	28.57(a_3)
Fe^{2+}	0.180(τ_1)	71.03(a_1)
	0.788(τ_2)	12.74(a_2)
	4.457(τ_3)	16.23(a_3)
Fe^{2+}–NO	0.191(τ_1)	37.02(a_1)
	0.788(τ_2)	38.68(a_2)
	3.707(τ_3)	24.30(a_3)

Table S3 Time constants and amplitudes for the population dynamics of ferric CBS at different pH. The excitation wavelength is 425nm

pH	Decay time (ps)	Amplitude
6.0	0.097(τ_1)	69.97(a_1)
	0.527(τ_2)	13.60(a_2)
	3.078(τ_3)	15.36(a_3)
6.2	0.127(τ_1)	52.37(a_1)
	0.608(τ_2)	22.30(a_2)
	4.015(τ_3)	25.31(a_3)
6.8	0.151(τ_1)	46.64(a_1)
	0.614(τ_2)	23.76(a_2)
	4.141(τ_3)	29.60(a_3)
7.0	0.221(τ_1)	42.76(a_1)
	0.715(τ_2)	22.41(a_2)
	4.327(τ_3)	34.83(a_3)
7.5	0.176(τ_1)	40.97(a_1)
	0.631(τ_2)	26.16(a_2)
	3.972(τ_3)	32.70(a_3)
8.0	0.140(τ_1)	47.82(a_1)
	0.593(τ_2)	23.45(a_2)
	3.784(τ_3)	28.57(a_3)
9.0	0.129(τ_1)	43.20(a_1)
	0.624(τ_2)	26.28(a_2)
	4.160(τ_3)	30.52(a_3)

References

(1) Taoka, S.; Banerjee, R. *J.Inorg.Biochem.* **2001**, *87*, 245-251.

(2) Green, E. L.; Taoka, S.; Banerjee, R.; Loehr, T. M. *Biochemistry* **2001**, *40*, 459-463.

(3) Guex, N.; Peitsch, M. C. *Electrophoresis* **1997**, *18*, 2714-2723.

(4) Puranik, M.; Nielsen, S. B.; Youn, H.; Hvitved, A. N.; Bourassa, J. L.; Case, M. A.; Tengroth, C.; Balakrishnan, G.; Thorsteinsson, M. V.; Groves, J. T.; McLendon, G. L.; Roberts, G. P.; Olson, J. S.; Spiro, T. G. *J.Biol.Chem* **2004**, *279*, 21096-21108.

(5) Puranik, M.; Weeks, C. L.; Lahaye, D.; Kabil, O.; Taoka, S.; Nielsen, S. B.; Groves, J. T.; Banerjee, R.; Spiro, T. G. *J.Biol.Chem.* **2006**, *281*, 13433-13438.

(6) Kumazaki, S.; Nakajima, H.; Sakaguchi, T.; Nakagawa, E.; Shinohara, H.; Yoshihara, K.; Aono, S. *J.Biol.Chem.* **2000**, *275*, 38378-38383.

(7) Rubtsov, I. V.; Zhang, T. Q.; Nakajima, H.; Aono, S.; Rubtsov, G. I.; Kumazaki, S.; Yoshihara, K. *J.Am.Chem.Soc.* **2001**, *123*, 10056-10062.

(8) Srajer, V.; Reinisch, L.; Champion, P. M. *J.Am.Chem.Soc.* **1988**, *110*, 6656-6670.

(9) Ye, X.; Ionascu, D.; Gruia, F.; Yu, A.; Benabbas, A.; Champion, P. M. *Proc.Natl.Acad.Sci.U.S A* **2007**, *104*, 14682-14687.

(10) Henry, E. R.; Sommer, J. H.; Hofrichter, J.; Eaton, W. A. *J.Mol.Biol.* **1983**, *166*, 443-451.

(11) Ye, X.; Yu, A. C.; Georgiev, G. Y.; Gruia, F.; Ionascu, D.; Cao, W. X.; Sage, J. T.; Champion, P. M. *J.Am.Chem.Soc.* **2005**, *127*, 5854-5861.